# Influences of Mono-Ni(P) and Dual-Cu/Ni(P) Plating on the Interfacial Microstructure Evolution of Solder Joints

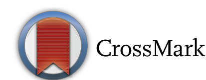

ZHE ZHANG, XIAOWU HU, XIONGXIN JIANG, and YULONG LI

The interfacial microstructures of Sn-3.0Ag-0.5Cu (SAC305) solder systems with thin Ni(P) mono-coatings and Cu-Ni(P) dual-coatings were investigated after reflowing and isothermal aging. The ultrathin mono-Ni(P) plating of the SAC305/Ni(P) solder joint was found to rapidly decompose and then transform into a $Ni_2SnP$ phase. An intermetallic compound (IMC) formed at the plating/substrate interface, indicating that the ultrathin mono-Ni(P) plating was not an effective diffusion barrier. However, only a single IMC layer ($(Cu,Ni)_6Sn_5$) formed at the solder/plating interface in the SAC305/Cu/Ni(P)/Cu system. The $(Cu,Ni)_6Sn_5$ IMC effectively suppressed atomic diffusion, protecting the Ni(P) plating and Cu substrate. Although P-Sn-O pores formed in the root of the $(Cu,Ni)_6Sn_5$ IMC layer, the dual-Cu/Ni(P) plating protected the solder system for an extended period. The IMC growth rate constants of the SAC305/Cu, SAC305/Ni(P), and SAC305/Cu/Ni(P)/Cu solder joint systems were 0.180, 0.342, and 0.068 $\mu$m/h$^{1/2}$, respectively. These results indicate that the application of dual-Cu/Ni(P) plating can effectively hinder the growth of IMC.

https://doi.org/10.1007/s11661-018-4983-7
© The Minerals, Metals & Materials Society and ASM International 2018

## I. INTRODUCTION

THE miniaturization of electronic equipment has led to the scale of solder joints decreasing accordingly. Solder/substrate interactions are important to the reliability of solder joints. Therefore, it is important to investigate the interfacial reactions between the solder and substrate.

Sn-Pb solders have been commonly used due to their excellent wetting properties, low melting points, and excellent mechanical properties.[1,2] However, the use of lead-free solders, such as those based on Sn-Bi and Sn-Ag, is increasing in response to environmental and health concerns.[3,4] Among these new solders, Sn-3.0Ag-0.5Cu (SAC305) alloy solder has become a very attractive choice for reflow soldering because of its excellent mechanical properties and solderability.[5–7]

The thickness of the intermetallic compound (IMC) is important to the solderability of a solder joint. The IMC must be thick enough to ensure strong, reliable bonding. However, an excessive thickness would adversely affect the reliability of the solder joint because of the brittleness of the IMC.[5,8–10]

Cu is the most common metal used in printed circuit boards (PCBs) because of its excellent conductivity. However, Cu oxidizes easily, and the resulting copper oxide reduces the solderability.[6] The electroless deposition of Ni(P) is commonly used to protect the Cu because of its good solder wettability and the low reaction rate between the Ni and Sn.[11–14] As a result of taking this approach, the interfacial reaction between the solder and the Ni(P) plating replaces the reaction between the solder and the substrate. Several Ni-containing IMCs, such as $Ni_3P$, $(Ni,Cu)_3Sn_4$, and $(Cu,Ni)_6Sn_5$ may form at the interface of a solder joint.[15–19] However, a Ni(P) coating, which is less than 5 $\mu$m thick, cannot act as an effective diffusion barrier between the solder and the Cu substrate.[20] Furthermore, the cost and signal stability limit the range of appropriate Ni(P) plating thicknesses.[6,21]

Liu and Wang reported that Cu–Sn IMCs can effectively suppress the diffusion of Ni atoms.[22,23] Thus, in the present study, an ultrathin Ni(P) film coated with a monolayer of Cu was used to replace the traditional Ni(P) coating. Unlike the Ni(P), the new dual-coating reduces the rate of the chemical reaction between the solder and the Ni(P) coating, thus prolonging the service life of the solder joint and improving the surface wettability. Lee *et al.* [24] reported that this Cu/Ni(P) dual-coating can prevent full-scale interaction

ZHE ZHANG, XIAOWU HU, XIONGXIN JIANG, and YULONG LI are with the Key Lab for Robot & Welding Automation of Jiangxi Province, Mechanical & Electrical Engineering School, Nanchang University, Nanchang 330031, P.R. China. Contact e-mails: huxiaowu@ncu.edu.cn; liyulong@ncu.edu.cn
Manuscript submitted January 15, 2018.
Article published online October 26, 2018

even at reaction temperatures exceeding 300 °C. In addition, the bonding strength of the Cu/Ni(P)/Sn three-dimensional solder joint was enhanced by the formation of a unique microstructure. However, the performance of this Cu/Ni(P) dual-coating during long-term thermal aging remains unknown.

There is, therefore, an urgent need to investigate the effect of this new dual-coating on the formation and growth behavior of IMC at the solder joint interface during thermal aging. Therefore, the present study set out to investigate the growth of the IMCs, the evolution of the interfacial microstructures, and the growth kinetics of the IMC layer in SAC305/Cu, SAC305/Ni(P)/Cu, and SAC305/Cu/Ni(P)/Cu systems.

## II. EXPERIMENTAL

In the present study, Cu pads were randomly divided into three groups, which were then used to explore the roles that different coatings play in the interfacial reactions between the Sn3.0Ag0.5Cu (SAC305) solder and the substrate. The groups were designated A (solder/Cu system), B (solder/Ni(P)/Cu system), and C (solder/Cu/Ni(P)/Cu system). One sample from each group was subjected to atomic force microscopy (AFM) to observe the surface of the coating. The AFM scanning area was $20 \times 20$ $\mu m^2$. All the Cu plates were ground with SiC sandpaper and polished with 0.25-$\mu$m diamond paste to ensure that the Cu substrates were as similar as possible to the PCBs used in actual production. Samples from groups B and C were first dried in alcohol and then placed in an Ni(P) plating solution at 80 °C for 1 hour to prepare the electroless Ni(P) coating. The concentration of P was approximately 15 at. pct and the resulting layer thickness was 0.8 $\mu$m. Then, the group C samples were put into a Cu plating solution at 40 °C for 5 minutes to produce a 2.7-$\mu$m Cu layer. The cross-sectional microstructure of the dual-coated Cu plate is shown in Figure 1. The chemical compositions of the plating baths used in the present study are listed in Tables I and II, respectively.

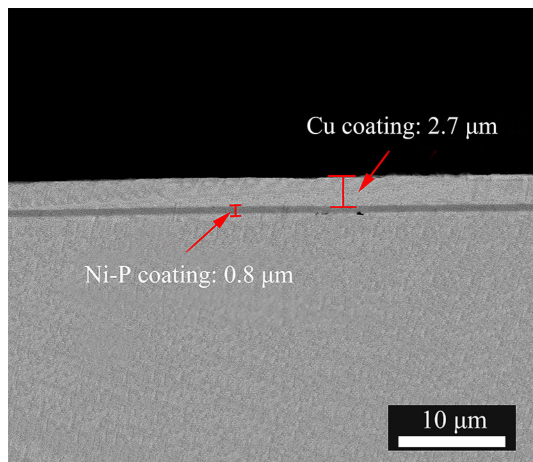


Fig. 1—SEM image of solder interface of dual-coated plate.

Lead-free SAC305 solder was used in the present study. The solder was placed on the center of each Cu plate. During the soldering process, the samples were passed through an infrared-enhanced conventional reflow oven. Although the melting point of SAC305 solder is 217 °C and reflow is typically performed at a temperature 30 °C higher than the melting point, the reflow temperature and time used in the present study were set to 280 °C and 10 minutes. As such, it was possible to form an appropriately thick IMC layer in very little time.[25–27] After cooling in air, the solder joints were isothermally aged at 150 °C for 24, 120, 240, and 360 hours in a box-type oven to observe the interfacial solid-state reactions of the solder joint during practical applications. Each specimen was divided into two parts by using an electrical discharge machine (EDM). One part was mounted in epoxy and polished to remove the surface layer and expose the cross-sectional microstructure, while the other part was immersed in a corrosive liquid and ultrasonicated to dissolve the residual solder and enable the observation of the grains.

Scanning electron microscopy (SEM) was used to examine the grain morphology. Energy dispersive spectroscopy (EDS) was used to examine the compositions of the IMCs. X-ray diffraction (XRD) was used to confirm the phases at the interface between the solder and substrate. A field-emission transmission electron microscope (FE-TEM) was employed to examine the microstructures of the IMC layer next to the substrate. The specimen for the TEM observation was prepared by using a focused ion beam (FIB) apparatus. The interfacial phases were identified by EDS combined with selected-area diffraction patterns (SADPs).

Adobe Photoshop was used to measure the thickness of the interfacial IMC, as follows: (a) the SEM image widths were gauged relative to the scale bar; (b) the total number of image pixels was recorded; (c) the number of pixels in the IMC was counted; (d) the IMC thickness was calculated using the following equation:

$$I = A/B \times C, \quad [1]$$

**Table I. Composition of Plating Bath for Electroless Ni(P)**

| Components of Plating Bath | Concentration |
|---|---|
| $NiSO_4 \cdot 6H_2O$ | 30 (g/L) |
| $NaH_2PO_2 \cdot H_2O$ | 35 (g/L) |
| $Na_3C_6H_5O_7 \cdot 2H_2O$ | 30 (g/L) |
| $NH_4Cl$ | 50 (g/L) |
| $CH_3CH(OH)COOH$ | 15 (ml/L) |

**Table II. Composition of Plating Bath for Electroplate Cu**

| Components of Plating Bath | Concentration |
|---|---|
| $Cu_2P_2O_7 \cdot 3H_2O$ | 100 (g/L) |
| $CuSO_4 \cdot 5H_2O$ | 50–75 (g/L) |
| $K_4P_2O_7 \cdot 3H_2O$ | 350 (g/L) |
| $K_2HPO_4 \cdot 3H_2O$ | 40–60 (g/L) |
| $H_2SO_4$ | 2–4 (g/L) |

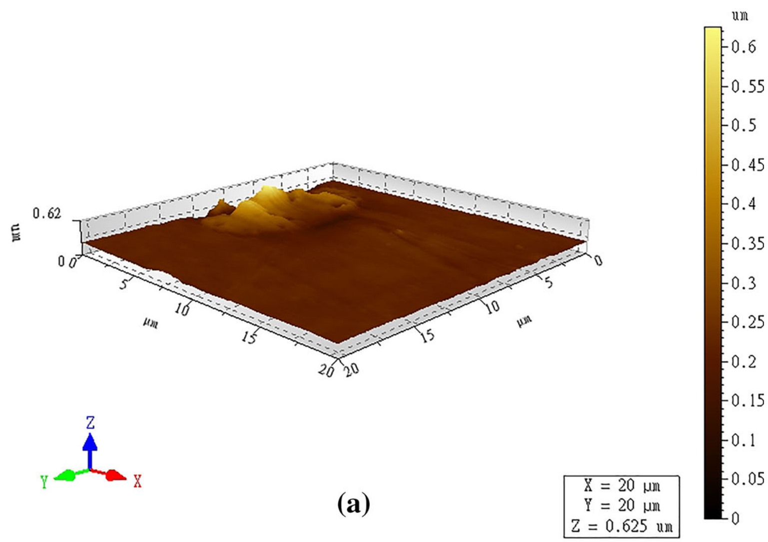


(a)

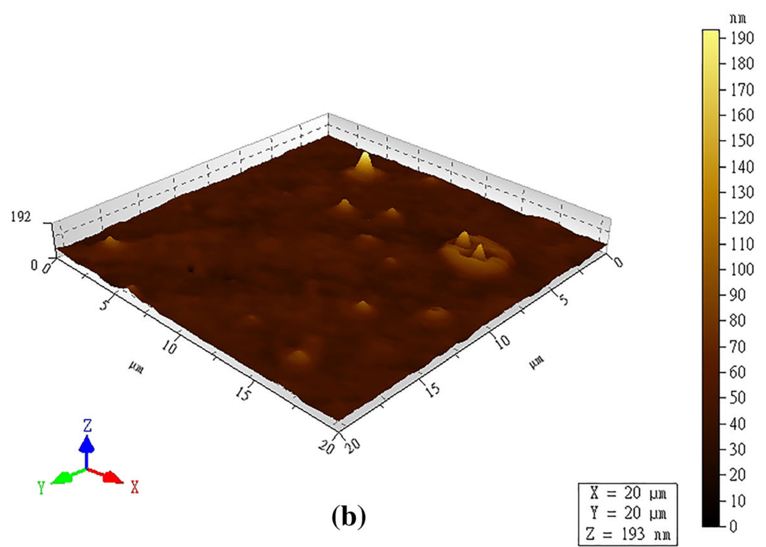


(b)

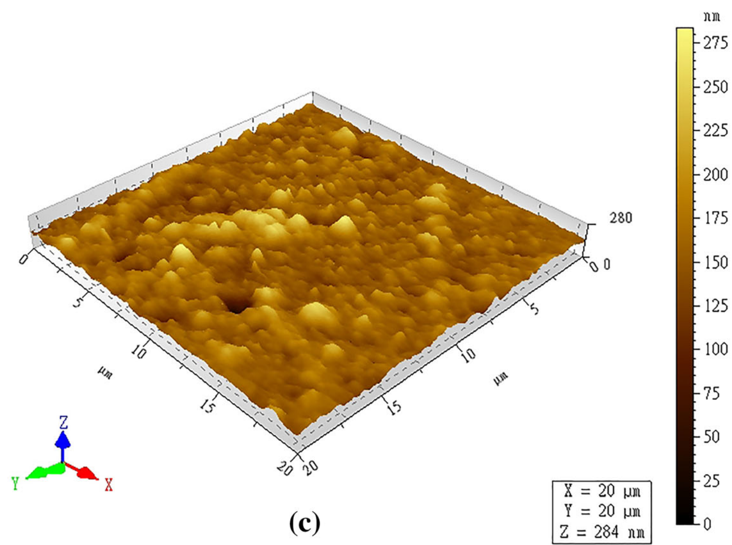


(c)

Fig. 2—AFM images of each system: (*a*) Cu, (*b*) Ni(P)/Cu, and (*c*) Cu/Ni(P)/Cu substrates.

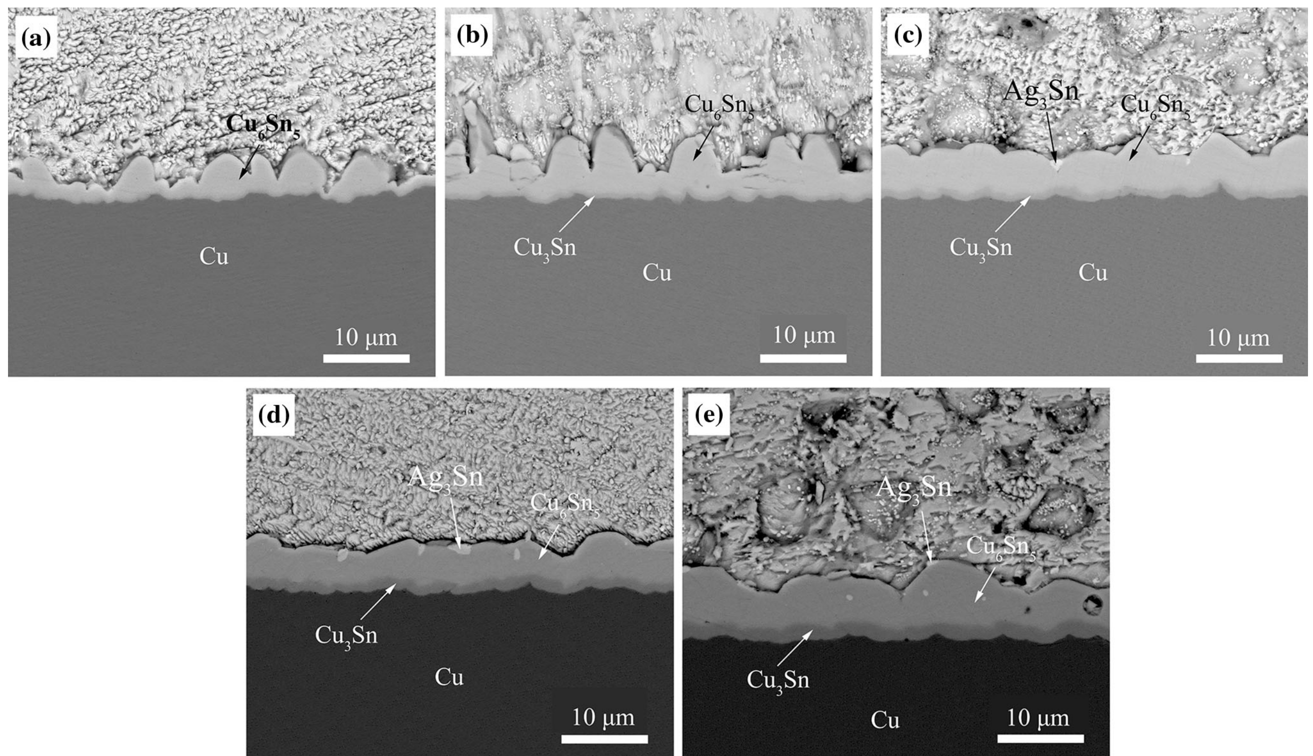


Fig. 3—Interfacial microstructures of SAC305/Cu system after aging for (*a*) 0 h, (*b*) 24 h, (*c*) 120 h, (*d*) 240 h, and (*e*) 360 h.

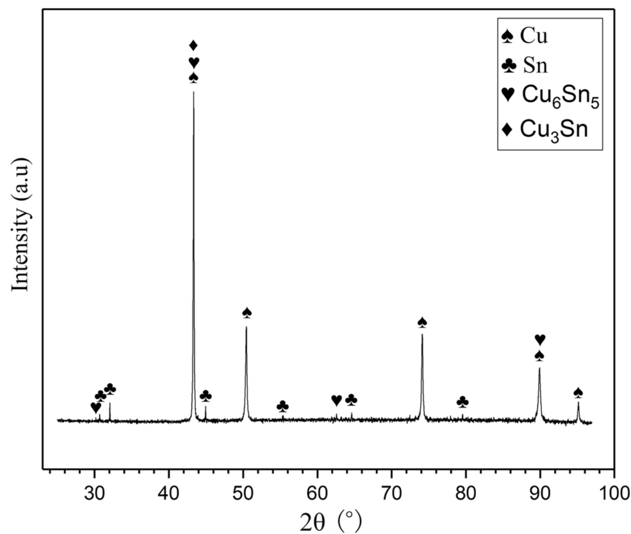


Fig. 4—XRD result for SAC305/Cu system after aging for 120 h.

where $I$ is the thickness of the IMC, $A$ is the number of pixels in the IMC, $B$ is the number of pixels in the image, and $C$ is the real height of the image.

## III. RESULTS AND DISCUSSION

Figure 2 shows AFM images of three types of substrates used in the present study. The surface roughness was indicated by the $R_z$ value. The $R_z$ values of the Cu, Ni(P)/Cu, and Cu/Ni(P)/Cu substrates were 625, 193, and 284 nm, respectively. The images show that most of the Cu and Ni(P)/Cu substrate surfaces are smooth, unlike that of the Cu/Ni(P)/Cu substrate. The Cu substrate exhibits a sparse, hilly shape, which might be the result of surface defects. During the formation of the Ni(P) coating, some of the grains crystallize *via* terrace-ledge-kink growth and form cones with a depth-to-width ratio of about 1.5:1 across the Ni(P)/Cu substrate. Instability in the electroplating current density causes the surface of the Cu/Ni(P)/Cu substrate to acquire irregular, dense humps. The depth-to-width ratio of these humps varies from 1:1 to 1:3. According to previous studies,[28,29] the current provides the energy required for nucleation. Thus, the deposition rate of Cu increases with the current density. This produces a compact, uniform and continuous surface. In addition, the sizes of the humps decrease as the current density increases. As pointed out by Quéré[30] and Liu *et al.*,[31] the solder wettability on the substrate is improved because the nanoscale substrate surface roughness reduces its equilibrium contact angle.

Figure 3 shows SEM images of the interfaces of the as-reflowed and isothermally aged solder/Cu systems. The phases in the solder joint were confirmed *via* XRD, as shown in Figure 4. Only a single layer of scalloped $Cu_6Sn_5$ IMC formed at the interface of the as-reflowed joint, as shown in Figure 3(a). As the isothermal aging time increased, the number of $Cu_6Sn_5$ scallops decreased but the thickness of the $Cu_6Sn_5$ IMC increased, as shown in Figures 3(b) through (e). Because the $Cu_6Sn_5$ IMC could prevent atoms from diffusing into the

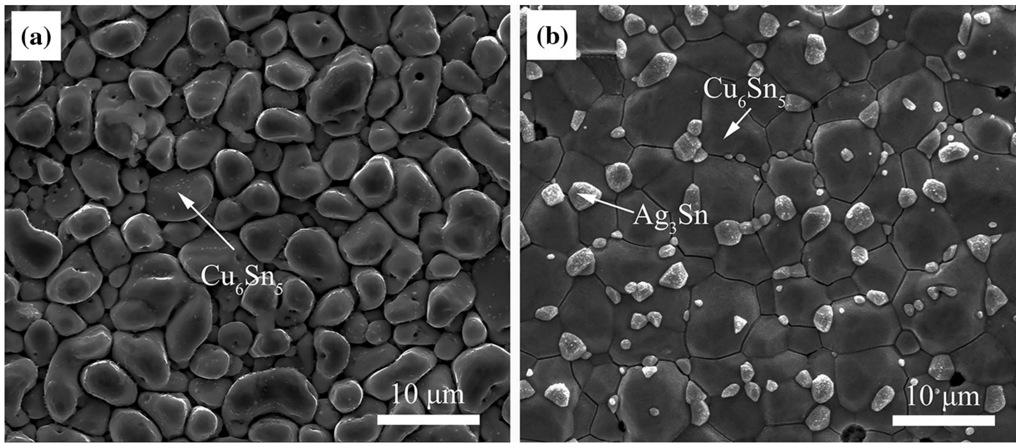


Fig. 5—Micrographs of SAC305/Cu system grains after aging for (*a*) 0 h and (*b*) 240 h.

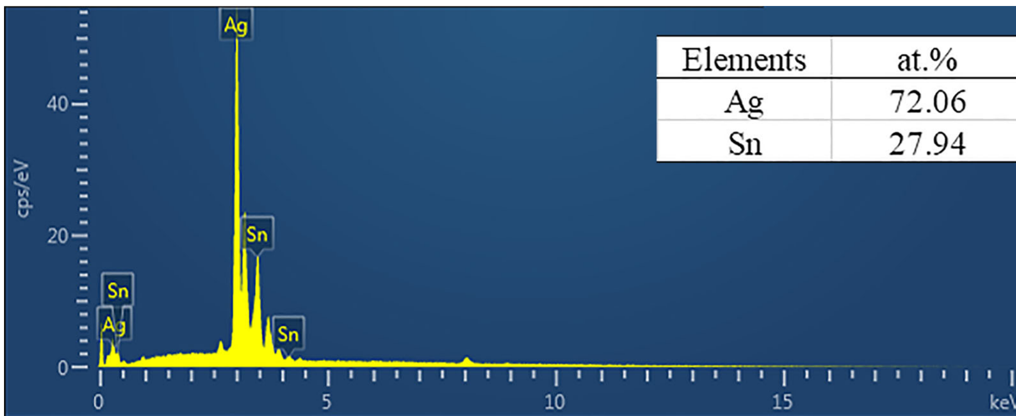


| Elements | at.% |
|---|---|
| Ag | 72.06 |
| Sn | 27.94 |

Fig. 6—EDS results for $Ag_3Sn$ grains in Fig. 5.

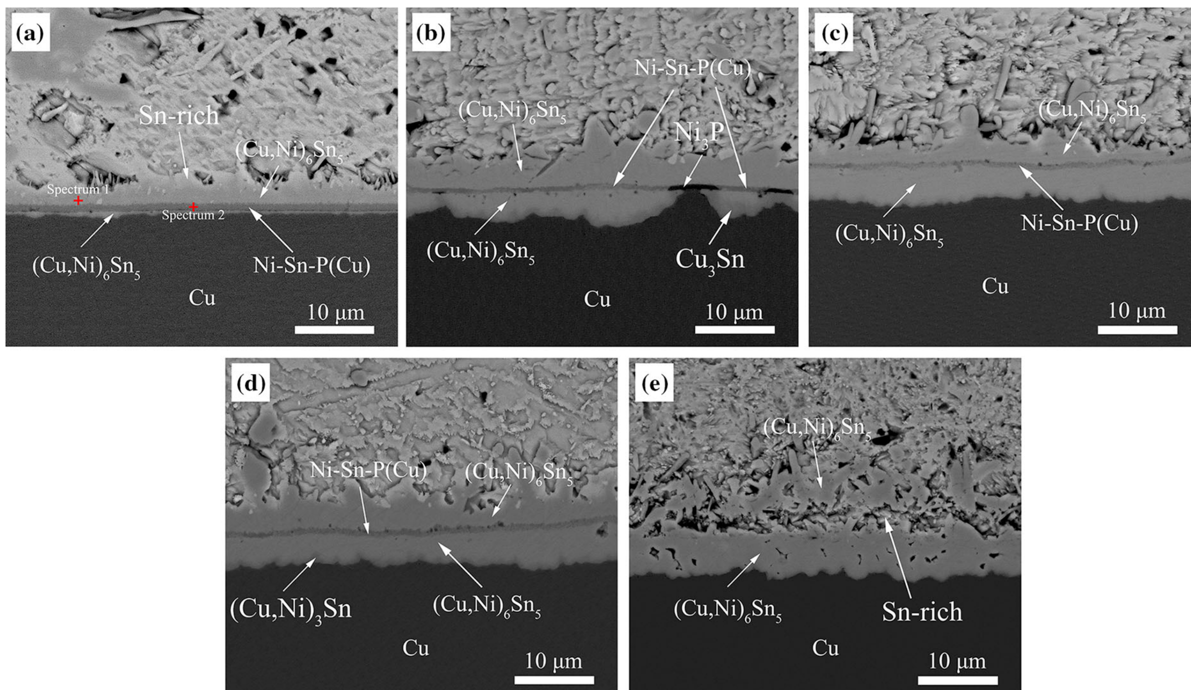


Fig. 7—Interfacial microstructure of SAC305/Ni(P) system after aging for (*a*) 0 h, (*b*) 24 h, (*c*) 120 h, (*d*) 240 h, and (*e*) 360 h.

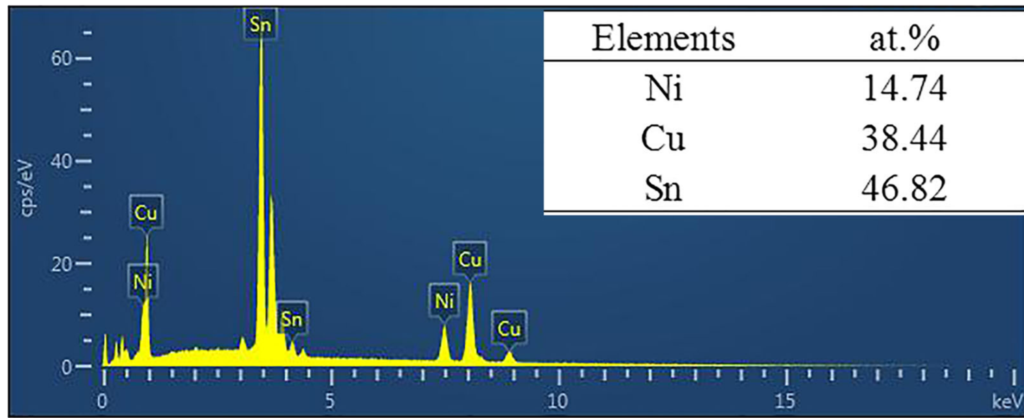


Fig. 8—EDS images of Spectrum 1 in Fig. 7(a).

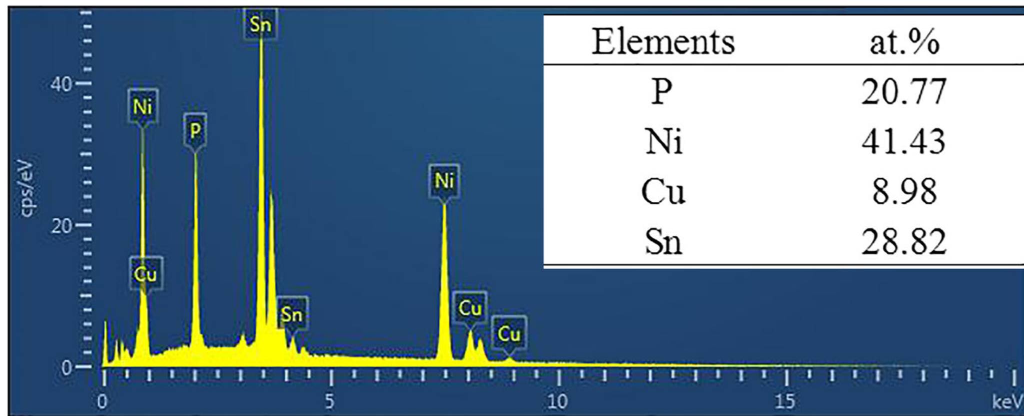


Fig. 9—EDS images of Spectrum 2 in Fig. 7(a).

IMC/substrate interface, the $Cu_3Sn$ IMC formed and grew between the $Cu_6Sn_5$ and Cu after isothermal storage for 24 hours. Furthermore, particle like $Ag_3Sn$ was observed after aging for 120 hours because of the chemical reaction between the Sn and Ag atoms from the solder, as shown in Figures 3(c) through (e). The dispersion of the $Ag_3Sn$ particles at the grain boundaries might enhance the solder joint strength due to dispersion strengthening.

It is well known that the process whereby interfacial IMC layers are formed can be described by the following equations:

$$6Cu + 5Sn \rightarrow Cu_6Sn_5 \quad [2]$$

$$3Cu + Sn \rightarrow Cu_3Sn \quad [3]$$

$$9Cu + Cu_6Sn_5 \rightarrow 5Cu_3Sn \quad [4]$$

When reflow begins, Cu atoms from both the substrate and the solder react with the Sn atoms to form the $Cu_6Sn_5$ IMC. Some $Cu_6Sn_5$ grains grow quickly and exhibit scalloped patterns in their cross sections, as shown in Figures 3(a) through (c). After long-term aging, the $Cu_6Sn_5$ IMC gradually becomes thick and dense, and thus can block atomic transport. As a result, fewer Cu and Sn atoms diffuse through this IMC layer. At the same time, Cu atoms from the solder react almost completely with the Sn atoms. Thus, the thickness of the $Cu_6Sn_5$ IMC grows slowly after aging for 120 hours, as shown in Figures 3(c) through (e). However, the growth of the as-formed $Cu_3Sn$ layer can take place at both the $Cu_6Sn_5/Cu_3Sn$ and $Cu_3Sn/Cu$ interfaces. Therefore, the $Cu_3Sn$ IMC continues to thicken after aging for 120 hours, as shown in Figures 3(c) through (e).

Figures 5(a) and (b) show SEM images of the interfacial $Cu_6Sn_5$ IMC grains in a solder/Cu system after reflowing and aging for 240 hours, respectively. During reflow, only a few $Cu_6Sn_5$ grains formed between the molten solder and Cu substrate. The $Cu_6Sn_5$ grains were observed to be pebble shaped with smooth surfaces. Spaces were observed between the grains, as shown in Figure 5(a). After aging, the pebble-shaped $Cu_6Sn_5$ grains grew by engulfing the other grains, to produce polygonal grains. The interstitial spaces between the grains disappeared. In addition, visibly dispersed $Ag_3Sn$ grains formed at the grain boundary, as shown in Figure 5(b). The $Ag_3Sn$ was

confirmed by EDS, as shown in Figure 6. These $Ag_3Sn$ grains may play a role in strengthening a solder joint. These results are all in good agreement with those of previous studies.[32,33]

Figure 7 shows SEM images of the interfaces of the as-reflowed and isothermally aged solder/Ni(P)/Cu systems. It was found that only a $(Cu,Ni)_6Sn_5$ IMC phase formed at the interface. At the initiation of reflow, the Ni(P) film coating limited the reaction rate between the solder and Cu substrate, as shown in Figure 7(a). The interaction between the solder and the Ni(P) coating is the first reaction in this system. The composition of the reaction product was 14.74 at. pct Ni, 38.44 at. pct Cu, and 46.82 at. pct Sn, as shown in Figure 8, suggesting that the IMC was $(Cu,Ni)_6Sn_5$. Between the $(Cu,Ni)_6Sn_5$ IMC layer and the Cu substrate, the Ni(P) plating transformed into $Ni_3P$ binary and a special Ni-Sn-P(Cu) layer, as shown in Figure 7(b). Park *et al.*[34] reported

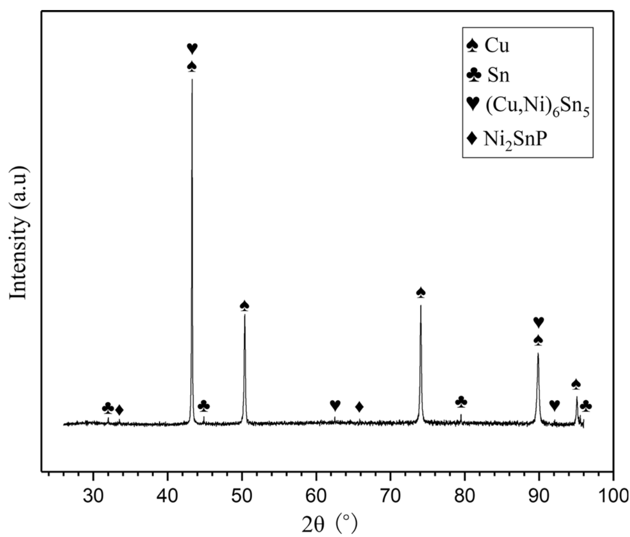


Fig. 10—XRD results of SAC305/Ni(P)/Cu system after aging for 120 h.

that, in a Sn-Ag/Au/Ni/Cu/Ti solder joint, the primary phase formed during the initial reaction stage is $Ni_3Sn_4$, containing a small amount of Cu. However, the mono-Ni(P) coating used in the present study was so thin that the $(Ni,Cu)_3Sn_4$ IMC did not form at the interface and therefore was not observed.

EDS was used to identify the composition of the Ni-Sn-P(Cu) layer. The EDS results show that the composition of the Ni-Sn-P(Cu) layer is 41.43 at. pct Ni, 28.82 at. pct Sn, 20.77 at. pct P, and 8.98 at. pct Cu, as shown in Figure 9. Numerous studies have revealed that several Ni-P compounds form at the solder/Ni(P) interface, such as $Ni_2P$, $Ni_2SnP$, $Ni_3P$, and $Ni_{12}P_5$.[15,16,19,35,36] Ho *et al.* used FE-EPMA to analyze the layer-type IMC in the SAC305/ultrathin-ENEPIG solder joint with a 0.31-$\mu$m Ni(P) layer and found that it contains 34.67 at. pct Sn, 6.71 at. pct Cu, 41.54 at. pct Ni, and 16.9 at. pct P. They confirmed that the phase was $Ni_2Sn_{1+x}P_{1-x}$.[37] Thus, it can be stated that the Ni-Sn-P(Cu) layer contains the $Ni_2SnP$ phase. The XRD results also demonstrate the presence of the $Ni_2SnP$ phase, as shown in Figure 10.

However, the high Cu content indicates that there may be another phase in the Ni-Sn-P(Cu) layer. An EDS line scan was acquired for the cross section of the solder/Ni(P)/Cu sample after aging for 24 hours to investigate the elemental depth profiles. The result is shown in Figure 11. It can be seen that the content of the Sn and Cu remains high in the $(Cu,Ni)_6Sn_5$ IMC layer. However, the Cu content in the Ni-Sn-P(Cu) layer decreases to a fixed value. Ho *et al.* also found the Ni-Sn-P(Cu) phase while also confirming that the Ni-Sn-P(Cu) layer was $Ni_2SnP$ with a certain amount of $(Cu,Ni)_6Sn_5$ at the grain boundaries.[20] Thus, it can be concluded that the high Cu content in the Ni-Sn-P(Cu) layer originates from the $(Cu,Ni)_6Sn_5$.

When the temperature rose to the melting point of the SAC305 solder, the Cu atoms in the solder reacted with the Sn atoms to form the $Cu_6Sn_5$ IMC at the solder/Ni(P) plating interface. Meanwhile, Ni atoms from the Ni(P) plating replaced some of the Cu atoms in the

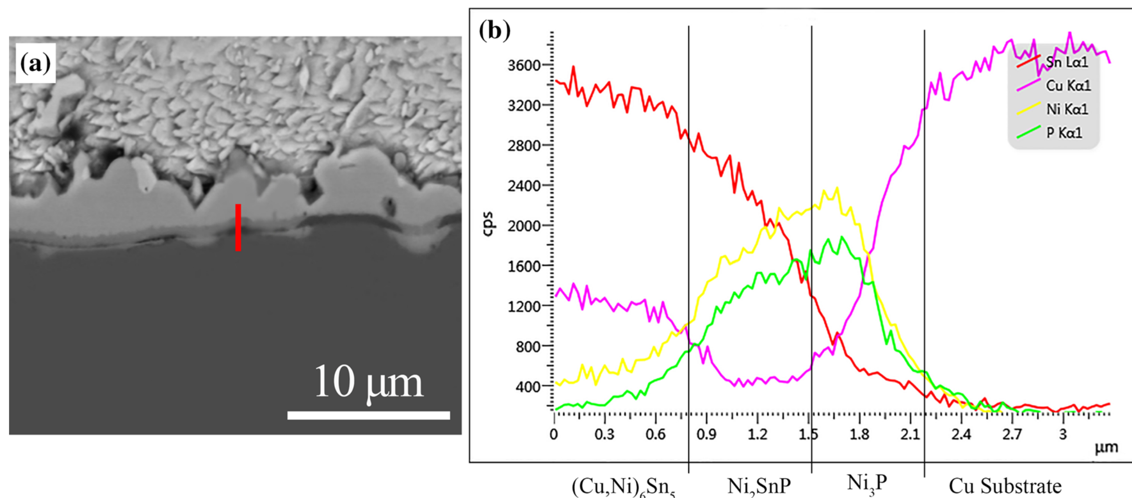


Fig. 11—(*a*) Sample of SAC305/Ni(P)/Cu solder system after aging for 24 h, (*b*) EDS line profiles showing element content across the line in (a).

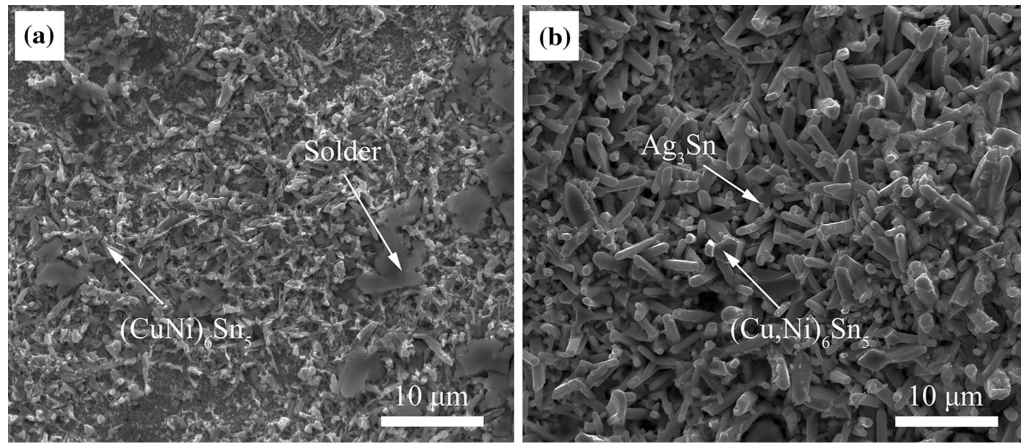


Fig. 12—Micrographs of grains in the SAC305/Ni(P) system after aging for (*a*) 0 h and (*b*) 120 h.

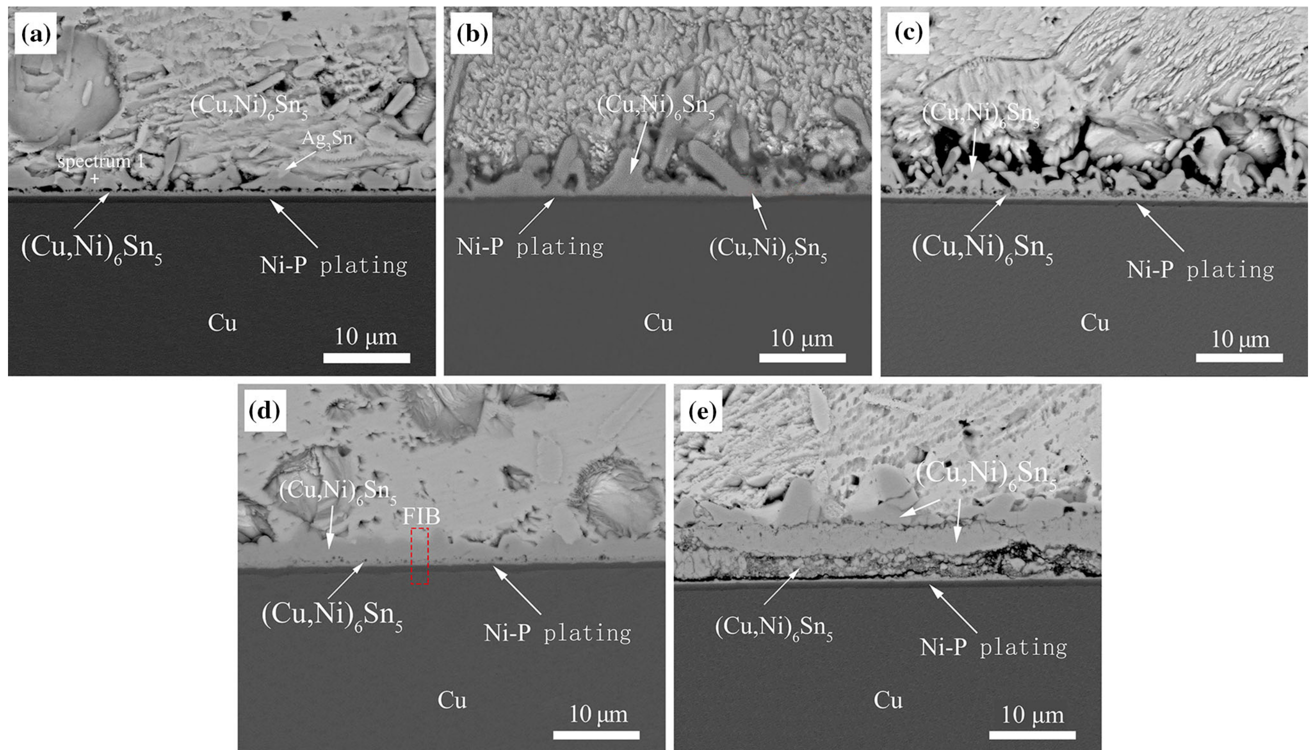


Fig. 13—Interfacial microstructure of SAC305/Cu/Ni(P)/Cu system after aging for (*a*) 0 h, (*b*) 24 h, (*c*) 120 h, (*d*) 240 h, and (*e*) 360 h.

$Cu_6Sn_5$ sublattice to form a $(Cu,Ni)_6Sn_5$ phase. In addition, the Ni(P) plating was so thin that it dissolved completely into the Sn-rich liquid to form a new liquid. This liquid contained large numbers of Ni and Sn atoms and became unstable at lower temperatures. During cooling, some regions of this liquid layer with high Ni atom concentrations transformed into a $Ni_3P$ layer, while the majority of this liquid layer formed a Ni-Sn-P layer containing a small amount of Cu.[38] This Ni-Sn-P(Cu) layer not only provided a solid substrate for $(Cu,Ni)_6Sn_5$ nucleation and growth, but also opened channels such that the molten solder could penetrate through to the Cu substrate.[21] The Sn atoms diffused to the Cu substrate alongside the Ni atoms to form a $(Cu,Ni)_6Sn_5$ IMC during isothermal aging. After aging for an extended period, the Ni atoms in the Ni-Sn-P(Cu) and $Ni_3P$ layers had completely diffused. Thus, the decomposition of the Ni-Sn-P(Cu) layer would result in the $(Cu,Ni)_6Sn_5$ IMC layer, which nucleated at the Ni-Sn-P(Cu) layer, separating from the existed $(Cu,Ni)_6Sn_5$ IMC layer close to the Cu substrate, as shown in Figure 7(e).

The Sn atoms diffused through the Ni-Sn-P(Cu) region and reacted with the Cu substrate to form a $Cu_6Sn_5$ IMC layer. In addition, a thin $Cu_3Sn$ IMC layer formed at the $Cu_6Sn_5$/Cu interface after aging for

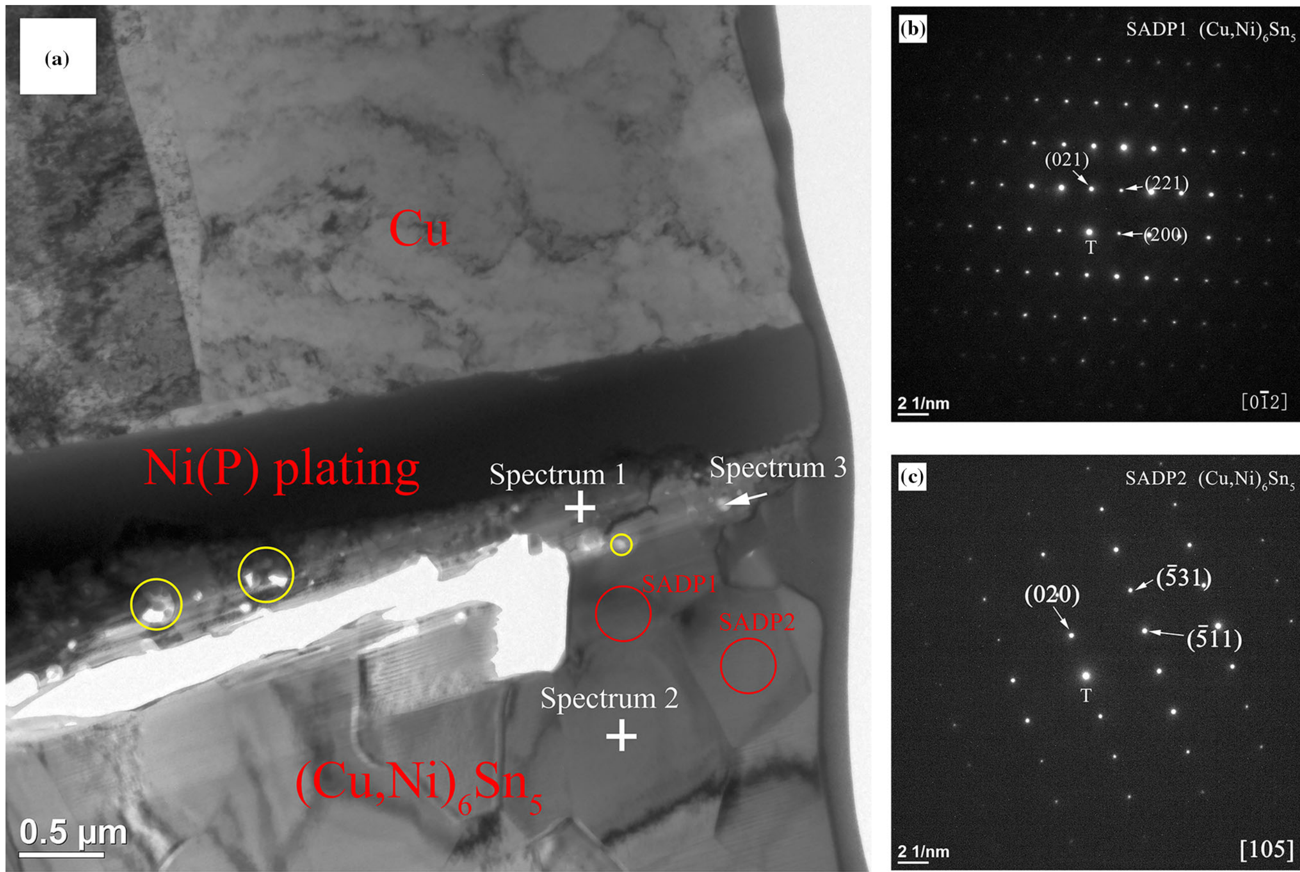


Fig. 14—(*a*) BF-TEM micrograph of IMC in Fig. 13(d), together with SADP of (Cu,Ni)6Sn5 (*b*) and (*c*).

**Table III. EDS Analysis Results of Phases Formed at SAC305/Cu/Ni(P)/Cu Interface, Shown in Fig. 14(a)**

| | Ni (At. Pct) | Cu | Sn | P | O |
|---|---|---|---|---|---|
| Spectrum 1 | 5.43 | 41.85 | 52.72 | — | — |
| Spectrum 2 | 2.90 | 49.85 | 47.25 | — | — |
| Spectrum 3 | — | 32.31 | 40.84 | 10.41 | 16.44 |

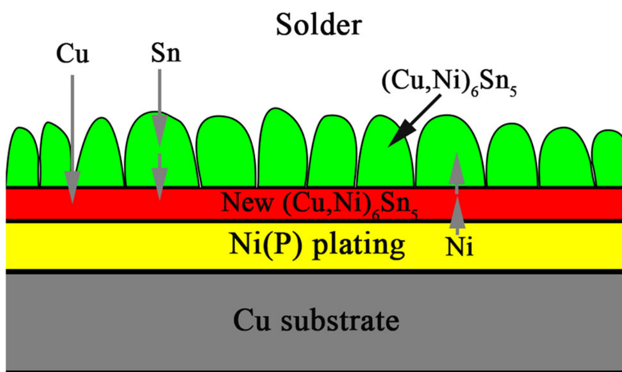


Fig. 15—Phase transformation in SAC/Cu/Ni(P) solder joint.

24 hours, as shown in Figure 7(b). However, more Sn atoms diffused through the Ni-Sn-P(Cu) layer as the $Ni_3P$ fully transformed into Ni-Sn-P(Cu). This thin $Cu_3Sn$ IMC layer then transformed into a $Cu_6Sn_5$ IMC layer, as shown in Figure 7(c). This process can be expressed by the following equation:

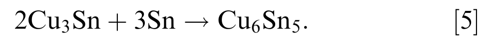

$$2Cu_3Sn + 3Sn \rightarrow Cu_6Sn_5. \quad [5]$$

Furthermore, the Cu substrate was well protected even before the complete transformation of the $Ni_3P$ layer into the Ni-Sn-P(Cu) layer. Thus, it can be concluded that a $Ni_3P$ layer would act as a superior diffusion barrier, relative to the Ni-Sn-P(Cu) layer.

After aging for 240 hours, the $(Cu,Ni)_3Sn$ IMC formed again at the $Cu_6Sn_5$/Cu interface because the thick $(Cu,Ni)_6Sn_5$ IMC prevented the Sn atoms from diffusing towards the Cu substrate. Thus, it can be concluded that both the $Ni_3P$ and $Cu_6Sn_5$ layers better prevent Sn diffusion than the Ni-Sn-P(Cu) layer. The Ni-Sn-P(Cu) layer dissolved after a long period of aging. The IMC layer that nucleated over the Ni-Sn-P(Cu) layer spalled from the IMC layer close to the Cu substrate, as shown in Figure 7(e). Meanwhile, the $Cu_3Sn$ compound dissolved again because the porous $(Cu,Ni)_6Sn_5$ layer cannot prevent Sn atoms from diffusing and reacting with the $(Cu,Ni)_3Sn$.

Figures 12(a) and (b) show the morphologies of the interfacial IMC grains in the solder/Ni(P)/Cu system after aging for 0 and 120 hours, respectively. The $(Cu,Ni)_6Sn_5$ grains formed first at the solder/Ni(P) interface, which presented irregular columns with a diameter of around 0.63 $\mu$m. The $(Cu,Ni)_6Sn_5$ grains

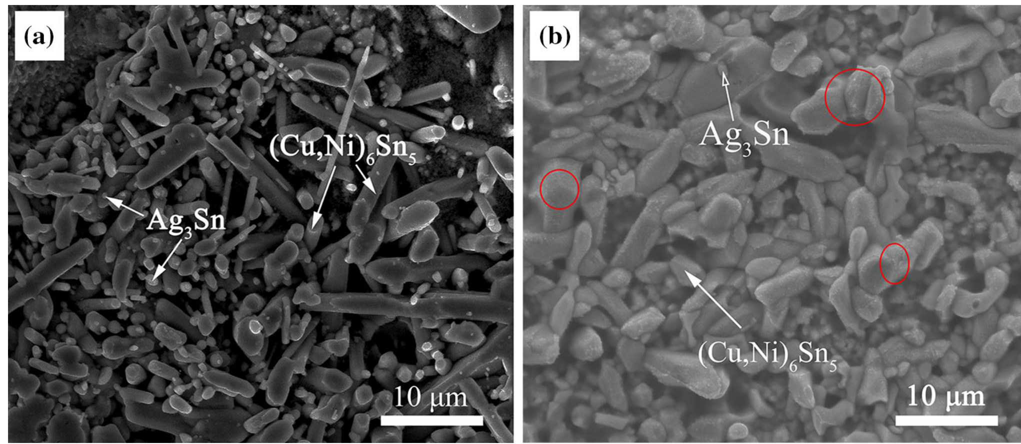


Fig. 16—Micrographs of grains in SAC305/Cu/Ni(P)/Cu system after aging for (*a*) 24 h and (*b*) 240 h.

**Table IV. Mean IMC Thickness of SAC305/Cu System During Aging**

| Aging Time (h) | 0 | 24 | 120 | 240 | 360 |
|---|---|---|---|---|---|
| IMC thickness ($\mu$m) | | | | | |
| $Cu_6Sn_5$ | 3.73 | 5.03 | 5.24 | 5.36 | 5.41 |
| $Cu_3Sn$ | — | 0.36 | 0.86 | 1.08 | 1.68 |

**Table V. Mean IMC Thicknesses of Three Systems Addressed in This Study During Aging**

| Aging Time (h) | 0 | 24 | 120 | 240 | 360 |
|---|---|---|---|---|---|
| Total IMC thickness ($\mu$m) | | | | | |
| SAC305/Cu system | 3.73 | 5.39 | 6.1 | 6.44 | 7.09 |
| SAC305/Ni(P) system | 4.26 | 6.55 | 7.65 | 9.55 | 11.08 |
| SAC305/Cu/Ni(P) system | 2.82 | 3.37 | 3.52 | 3.97 | 4.16 |

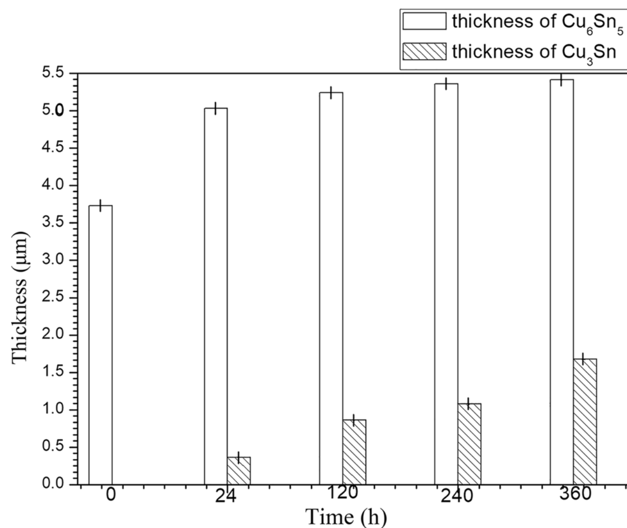


Fig. 17—Thicknesses of IMC in SAC305/Cu system after aging for different durations.

were arranged both randomly and close together. However, after aging for 120 hours, those grains for which the growth direction was perpendicular to the substrate grew faster than the others, resulting in the small grains being engulfed by the large grains. The vertically grown grains caused the surfaces in the cross sections shown in Figures 7(c) and (d) to exhibit rough interfaces. In addition, the reliability of the solder joint may be compromised by the voids between the intersecting grains.

Figure 13 shows SEM images of the solder/Cu/Ni(P)/Cu system interface after reflowing and aging for different durations. By means of EDS, the composition of Spectrum 1 in Figure 13(a) was determined to be 8.16 at. pct Ni, 43.22 at. pct Cu, and 48.62 at. pct Sn, corresponding to $(Cu,Ni)_6Sn_5$. The $(Cu,Ni)_6Sn_5$ had a plate shape prior to the thermal aging for 120 h. After aging for 120 hours, however, the Cu plating was found to have been completely consumed, while the plate-shaped $(Cu,Ni)_6Sn_5$ being transformed into a scallop shape. In addition, it was observed that two IMC layers formed between the solder and the Ni(P) plating, as shown in Figures 13(a) and (d). TEM was used to investigate the phase formed next to the Ni(P) plating. This is discussed in detail in the following section.

Figure 14 shows a bright-field TEM image, together with an enlarged view of the $(Cu,Ni)_6Sn_5$/Ni(P) interface, indicated by the rectangle in Figure 13(d). The elemental compositions of Spectrums 1 and 2 in Figure 14(a) were confirmed *via* TEM-EDS, as listed in Table III. Thus, it could be concluded that only $(Cu,Ni)_6Sn_5$ IMC formed between the solder and the Ni(P) plating. The electron diffraction pattern confirmed that the $(Cu,Ni)_6Sn_5$ exhibited a $Cu_6Sn_5$ crystal structure, as indicated by SADP1 and SADP2 in Figures 14(b) and (c).

Figure 15 is a schematic diagram illustrating the phase formation and atomic fluxes of Ni, Cu, and Sn through the reaction zone of the solder/Ni(P), explaining the formation of the two $(Cu,Ni)_6Sn_5$ layers. As the temperature rose to the melting point of the SAC305 solder, the Sn atoms reacted with the Cu atoms from the

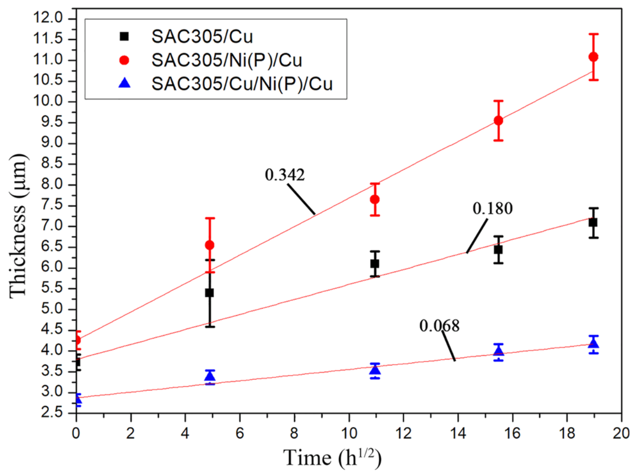


Fig. 18—Relationship between square root of aging time and IMC layer thickness in the solder systems in this study.

Cu coating to form the $Cu_6Sn_5$ IMC. Meanwhile, Ni atoms from the Ni(P) plating diffused into the $Cu_6Sn_5$ IMC and replaced some of the Cu atoms in the $Cu_6Sn_5$ sublattice to form $(Cu,Ni)_6Sn_5$. In addition, Cu and Sn atoms from the solder diffused through the grain boundaries of the $(Cu,Ni)_6Sn_5$ and reacted with Ni from the Ni(P) plating to form another $(Cu,Ni)_6Sn_5$ IMC. This $(Cu,Ni)_6Sn_5$ nucleated on the Ni(P) plating where it exhibited poor wettability relative to the upper $(Cu,Ni)_6Sn_5$.

Numerous pore-like defects formed in the root of the $(Cu,Ni)_6Sn_5$ layer, as shown in Figure 14(a). The elemental composition of the pore was confirmed to be 10.41 at. pct P, 16.44 at. pct O, 32.31 at. pct Cu, and 40.84 at. pct Sn, as listed in Table III. These pores had been identified in previous studies.[39,40] Ho *et al.* reported that the pores exhibit an amorphous structure and may result in the $(Cu_{0.6}Ni_{0.4})_6Sn_5$ spalling from the second $Cu_6Sn_5$ layer.[40]

It is clear that the upper $(Cu,Ni)_6Sn_5$ IMC layer spalls from the lower $(Cu,Ni)_6Sn_5$ IMC layer after aging for 360 h, as shown in Figure 13(e). There are two possible explanations for this spalling. The first is the low concentration of Cu in the solder. Chen *et al.* found that, when the Cu concentration in Sn-Cu based solder fell to a critical threshold, the $(Cu,Ni)_6Sn_5$ next to the solder was thermodynamically unstable, which resulted in the $(Cu,Ni)_6Sn_5$ spalling from the interface and thus making room for the nucleation and growth of another stable phase.[41] Another possible explanation is the poor wetting between the two $(Cu,Ni)_6Sn_5$ layers. Tu *et al.* reported that the poor wetting between the $Cu_6Sn_5$ and Cr-O in the solder/Cu/Cu-Cr solder joint caused spalling of the $Cu_6Sn_5$ grains into the molten solder.[42]

The Ni(P) coating of the SAC305/Cu/Ni(P)/Cu solder system was barely consumed during the present study. When the solder/Cu/Ni(P)/Cu system operates at a relatively low temperature over an extended duration, the solder joint interface can be regarded as being similar to that shown in Figure 13(d). Therefore, it can be confirmed that a Cu/Ni(P) dual-coating can effectively protect the substrate even when the Ni(P) coating is thin.

Figures 16(a) and (b) show the morphologies of the interfacial IMC grains in the solder/Cu/Ni(P)/Cu system after aging for 24 and 120 hours, respectively. Columnar $(Cu,Ni)_6Sn_5$ and $Ag_3Sn$ grains can be clearly observed. The average diameter of the resulting $(Cu,Ni)_6Sn_5$ grains is approximately 1 $\mu$m and the underlying Ni(P) plating is smooth. The size and diameter of the grains increased from 1 to 2.95 $\mu$m with the aging time. These grains grew by engulfing neighboring grains, as confirmed by the disappearance of the grain boundaries indicated by the circles in Figure 16(b). After aging for 240 hours, the $(Cu,Ni)_6Sn_5$ grains grew dense such that the underlying Ni(P) plating could not be observed. This dense distribution of grains could suppress the continued diffusion of the Ni atoms from the Ni(P) plating and their reaction with the solder.

To investigate the IMC growth kinetics, the thicknesses of the $Cu_6Sn_5$ and $Cu_3Sn$ IMCs in the SAC305/Cu system were measured by applying Eq. [1]. The results are listed in Table IV and shown in Figure 17. It can be seen that the $Cu_6Sn_5$ IMC is at least three times thicker than the $Cu_3Sn$ IMC. After aging for 24 hours, the $Cu_6Sn_5$ IMC is so thick that it prevents the diffusion of Sn atoms. Thus, the $Cu_3Sn$ IMC forms at the $Cu_6Sn_5$/Cu interface. As seen from the figure, the $Cu_6Sn_5$ IMC layer grows more slowly than the $Cu_3Sn$ IMC layer. This may be a result of the following: the thick $Cu_6Sn_5$ IMC layer may prevent the Cu atoms from diffusing into the solder/$Cu_6Sn_5$ interface such that the $Cu_3Sn$ phase is formed both at the solder/$Cu_6Sn_5$ and the $Cu_6Sn_5$/Cu interfaces. In other words, the $Cu_3Sn$ layer grows in two directions, while the $Cu_6Sn_5$ layer grows only in one. These results are similar to those presented by Peng *et al.*[43]

The thickness of the IMC layer that grows during aging can be expressed by the following equation[44]:

$$Y = At^n + B, \quad [6]$$

where $Y$ is the thickness of the IMC layer at time $t$, $B$ is the initial thickness of the IMC layer after soldering, $A$ is the IMC growth rate constant, and $n$ is the time exponent.

The IMC growth of these three solder systems follows a parabolic pattern. According to Kim *et al.*, the growth of IMCs generally follows a linear or parabolic pattern during solid-state aging. The growth rate is governed by the reaction rate at the growth site when the intermetallic growth conforms to linear kinetics, whereas parabolic growth kinetics imply that intermetallic growth is controlled by volume diffusion.[45] Although Liang *et al.* reported that the IMC growth method conforms to the power law equation when aged at a temperature near the melting point for an extended duration,[25] the IMC growth in this study follows a parabolic curve, implying that the value of $n$ is 0.5.

Because of the complexity of the interfacial reaction layers in the SAC305/Ni(P)/Cu and SAC305/Cu/Ni(P)/Cu systems during aging, only the total thicknesses of the IMC layers in these systems were recorded. The

results are listed in Table V. The total thickness of the SAC305/Ni(P)/Cu system IMC layer is 1.5 times greater than that observed for the SAC305/Cu system and three times greater than that of the SAC305/Cu/Ni(P)/Cu system. The total thickness of the SAC305/Cu system IMC layer is greater than that observed in the SAC305/Cu/Ni(P)/Cu system. The thinnest IMC in the SAC305/Cu/Ni(P)/Cu system shows that the Cu/Ni(P) coating effectively prevents IMC growth even when the Ni(P) coating is thin.

Figure 18 shows the IMC thickness as a function of the square root of the aging time. The slopes of the curves represent the values of $A$. The $A$ values of the SAC305/Cu, SAC305/Ni(P)/Cu, and SAC305/Cu/Ni(P)/Cu solder systems are 0.180, 0.342, and 0.068 $\mu m/h^{1/2}$, respectively. This indicates that the dual-Cu/Ni(P) coating can prevent IMC growth when the plating is quite thin. It can thus be concluded that the dense $(Cu,Ni)_6Sn_5$ of the SAC305/Cu/Ni(P)/Cu solder system is an excellent diffusion barrier. Growth occurs in only one direction in the SAC305/Cu/Ni(P)/Cu system.

The rapid IMC growth in the SAC305/Ni(P)/Cu solder system may have several causes. One possibility is that the Ni-Sn-P(Cu) layer is not an efficient diffusion barrier. If this was the case, Sn atoms from the solder would diffuse into the Ni(P)/Cu interface and react with the Cu substrate to form Cu–Sn compounds. Another possibility is supported by the EDS image of the Ni-Sn-P(Cu), shown in Figure 9. The Ni-Sn-P(Cu) layer has a high Sn atom content, and thus could be regarded as being another source of Sn atom diffusion. Thus, the Cu-Sn alloy IMC forms simultaneously at the solder/Ni(P) and Ni(P)/Cu interfaces.

The second data point of the SAC305/Cu and SAC305/Ni(P) systems, shown in Figure 18, clearly deviates from the fitted line. In other words, the IMC thicknesses observed in the SAC305/Cu and SAC305/Ni(P)/Cu systems after aging for 24 hours are clearly higher than expected. This phenomenon might be a result of the rapid reaction that occurs between the solder and substrate when there is no protective layer such as the dense $Cu_6Sn_5$ IMC layer.

## IV. CONCLUSIONS

Intermetallic compound formation in SAC305/Cu, SAC305/Ni(P)/Cu, and SAC305/Cu/Ni(P)/Cu solder systems was investigated during reflowing at 280 °C and isothermal aging at 150 °C. The following conclusions could be drawn:

(a) The IMC growth observed in the present study conforms to parabolic growth kinetics, indicating that the IMC growth is controlled by volume diffusion. However, a thick $Cu_6Sn_5$ IMC would prevent Sn atoms from diffusing through it to form a $Cu_3Sn$ layer. The $Cu_6Sn_5$ layer grew more slowly than the $Cu_3Sn$ layer because part of the $Cu_6Sn_5$ IMC was transformed to a $Cu_3Sn$ IMC through the reaction between the $Cu_6Sn_5$ and Cu.

(b) A thin Ni(P) coating was not an effective diffusion barrier. Both Cu and Sn atoms could diffuse through the thin Ni(P) coating, and thus Cu-Sn IMCs were detected at the both the solder/Ni(P) and Ni(P)/Cu interfaces. In contrast, the $Ni_3P$ phase and $Cu_6Sn_5$ IMC were better barriers than the Ni-Sn-P(Cu) layer. In addition, the $Cu_3Sn$ IMC could transform into a $Cu_6Sn_5$ IMC when the Sn atomic content was sufficient. In addition, the Ni(P) coating dissolved completely after an extended aging period, causing the IMC layer to detach from the underlying IMC layer.

(c) The Cu/Ni(P) dual-coating more effectively prevented atomic diffusion than the Ni(P) mono-coating. Thus, Cu–Sn IMCs grew only at the solder/plating interface. Two $(Cu,Ni)_6Sn_5$ IMC layers formed between the solder and the Ni(P) plating. The $(Cu,Ni)_6Sn_5$ layer next to the substrate resulted from the interaction between the Cu and Sn originating from the solder and Ni(P) plating. In addition, the low Cu concentration in the solder and the poor wetting between the two $(Cu,Ni)_6Sn_5$ layers resulted in the upper $(Cu,Ni)_6Sn_5$ layer detaching from the lower $(Cu,Ni)_6Sn_5$ layer.

(d) After isothermal aging under the same conditions, the growth rate constants of the SAC305/Cu, SAC305/Ni(P), and SAC305/Cu/Ni(P)/Cu solder systems were found to be 0.180, 0.342, and 0.068 $\mu m/h^{1/2}$, respectively. It was confirmed that the dual-Cu/Ni(P) plating is more effective than the mono-Ni(P) plating at preventing Sn and Cu atom diffusion during solid-state aging.


## ACKNOWLEDGMENTS

This study was supported by the Nature Science Foundation of China (No. 51465039, 51765040), and the Nature Science Foundation of Jiangxi Province (20161BAB206122).


## REFERENCES


1. J.W. Nah, J.H. Kim, H.M. Lee, and K.W. Paik: *Acta Mater.*, 2004, vol. 52, pp. 129–36.
2. Y. Ding, C.Q. Wang, Y.H. Tian, and B.B. Zhang: *Metall. Mater. Trans. A*, 2006, vol. 37A, pp. 1017–25.
3. V. Kumar, Z.Z. Fang, J. Liang, and N. Dariavach: *Metall. Mater. Trans. A*, 2006, vol. 37A, pp. 2505–14.
4. X. Gu, K.C. Yung, Y.C. Chan, and D. Yang: *J. Mater. Sci.*, 2011, vol. 22, pp. 217–22.
5. D.G. Kim, J.W. Kim, and S.B. Jung: *Mater. Sci. Eng. B*, 2005, vol. 121, pp. 204–10.
6. S.R.A. Idris: Ph.D. Dissertation, University Teknologi Malaysia, 2008.
7. P. Sungkhaphaitoon and T. Plookphol: *Metall. Mater. Trans. A*, 2018, vol. 49A, pp. 652–60.
8. A. Sharif, M.N. Islam, and Y.C. Chan: *Mater. Sci. Eng. B*, 2004, vol. 113, pp. 184–89.
9. H.T. Lee, M.H. Chen, H.M. Jao, and T.L. Liao: *Mater. Sci. Eng. A*, 2003, vol. 358, pp. 134–41.

10. L. Meinshausen: Ph.D. Dissertation, Electronics. University de Bordeaux, 2014.
11. J. Yu and K. Kim: *Metall. Mater. Trans. A*, 2015, vol. 46A, pp. 3173–81.
12. S. Eraslan and M. Ürgen: *Surf. Coat. Technol.*, 2015, vol. 265, pp. 46–52.
13. K.N. Braszczyńska-Malik and J. Kamieniak: *Metall. Mater. Trans. A*, 2017, vol. 48A, pp. 5649–57.
14. T.R. Tamilarasan, R. Rajendran, G. Rajagopal, and J. Sudagar: *Surf. Coat. Technol.*, 2015, vol. 276, pp. 320–26.
15. Y.C. Lin and J.G. Duh: *Scripta Mater.*, 2006, vol. 54, pp. 1661–65.
16. Y.C. Lin, T.Y. Shih, S.K. Tien, and J.G. Duh: *Scripta Mater.*, 2007, vol. 56, pp. 49–52.
17. Y.C. Lin, K.J. Wang, and J.G. Duh: *J. Electron. Mater.*, 2010, vol. 39, pp. 283–94.
18. S.P. Peng, W.H. Wu, C.E. Ho, and Y.M. Huang: *J. Alloys Compd.*, 2010, vol. 493, pp. 431–37.
19. W.H. Wu, C.S. Lin, S.H. Huang, and C.E. Ho: *J. Electron. Mater.*, 2010, vol. 39, pp. 2387–96.
20. C.E. Ho, C.W. Fan, and W.Z. Hsieh: *Surf. Coat. Technol.*, 2014, vol. 259, pp. 244–51.
21. C.Y. Ho, J.G. Duh, C.W. Lin, C.J. Lin, and Y.H. Wu: *J. Mater. Sci.*, 2013, vol. 48, pp. 2724–32.
22. C.Y. Liu and S.J. Wang: *J. Electron. Mater.*, 2003, vol. 32, pp. 1303–09.
23. S.J. Wang and C.Y. Liu: *Scripta Mater.*, 2003, vol. 49, pp. 813–18.
24. B. Lee, H. Jeon, K.W. Kwon, and H.J. Lee: *Acta Mater.*, 2013, vol. 61, pp. 6736–42.
25. J. Liang, N. Dariavach, P. Callahan, and D. Shangguan: *Mater. Trans.*, 2006, vol. 47, pp. 317–25.
26. P. Chen, X. Zhao, Y. Wang, Y. Liu, H. Li, and Y. Gu: *J. Mater. Sci.*, 2015, vol. 26, pp. 1940–49.
27. X. Hu, T. Xu, L.M. Keer, Y. Li, and X. Jiang: *J. Alloys Compd.*, 2017, vol. 690, pp. 720–29.
28. M. Haerifar and M. Zandrahimi: *Appl. Surf. Sci.*, 2013, vol. 284, pp. 126–32.
29. C.W. Liu, Y.L. Wang, M.S. Tsai, H.P. Feng, and S.C. Chang: *J. Vac. Sci. Technol. A*, 2005, vol. 23, pp. 658–62.
30. D. Quéré: *Annu. Rev. Mater. Res.*, 2008, vol. 38, pp. 71–99.
31. W. Liu and D.P. Sekulic: *Langmuir*, 2011, vol. 27, pp. 6720–30.
32. J.W. Yoon and S.B. Jung: *J. Mater. Sci.*, 2004, vol. 39, pp. 4211–17.
33. P.T. Vianco, J.A. Rejent, and P.F. Hlava: *J. Electron. Mater.*, 2004, vol. 33, pp. 991–1004.
34. J.Y. Park, C.W. Yang, J.S. Ha, C.U. Kim, E.J. Kwon, S.B. Jung, and C.S. Kang: *J. Electron. Mater.*, 2001, vol. 30, pp. 1165–70.
35. C.Y. Ho, J.G. Duh, C.W. Lin, C.J. Lin, Y.H. Wu, H.C. Hong, and T.H. Wang: *J. Mater. Sci.*, 2013, vol. 48, pp. 2724–32.
36. Y.C. Lin, K.J. Wang, and J.G. Duh: *J. Electron. Mater.*, 2010, vol. 39, pp. 283–94.
37. C.Y. Ho and J.G. Duh: *Mater. Chem. Phys.*, 2014, vol. 148, pp. 21–27.
38. V. Vuorinen, T. Laurila, H. Yu, and J.K. Kivilahti: *J. Appl. Phys.*, 2006, vol. 99, pp. 3530–36.
39. Z. Chen, A. Kumar, and M. Mona: *J. Electron. Mater.*, 2006, vol. 35, pp. 2126–34.
40. C.E. Ho, C.W. Fan, W.H. Wu, and T.T. Kuo: *Thin Solid Films*, 2013, vol. 529, pp. 364–48.
41. W.M. Chen, S.C. Yang, M.H. Tsai, and C.R. Kao: *Scripta Mater.*, 2010, vol. 63, pp. 47–49.
42. K.N. Tu and K. Zeng: *Mater. Sci. Eng. R*, 2001, vol. 34, pp. 1–58.
43. W. Peng, E. Monlevade, and M.E. Marques: *Microelectron. Reliab.*, 2007, vol. 47, pp. 2161–68.
44. J. Shen, M. Zhao, P. He, and Y. Pu: *J. Alloys Compd.*, 2013, vol. 574, pp. 451–58.
45. D.G. Kim and S.B. Jung: *J. Alloys Compd.*, 2005, vol. 386, pp. 151–56.